

Topological Defects: Origin of Nanopores and Enhanced Adsorption Performance in Nanoporous Carbon

Junjie Guo, James R. Morris, Yungok Ihm, Cristian I. Contescu, Nidia C. Gallego, Gerd Duscher, Stephen J. Pennycook, and Matthew F. Chisholm*

A scanning transmission electron microscopy investigation of two nanoporous carbon materials, wood-based ultramicroporous carbon and poly(furfuryl alcohol)-derived carbon, is reported. Atomic-resolution images demonstrate they comprise isotropic, three-dimensional networks of wrinkled one-atom-thick graphene sheets. In each graphene plane, nonhexagonal defects are frequently observed as connected five- and seven-atom rings. Atomic-level modeling shows that these topological defects induce localized rippling of graphene sheets, which interferes with their graphitic stacking and induces nanopores that lead to enhanced adsorption of H_2 molecules. The poly(furfuryl alcohol)-derived carbon contains larger regions of stacked layers, and shows significantly smaller surface area and pore volume than the ultramicroporous carbon.

1. Introduction

A variety of novel structures can be constructed with carbon atoms, stemming not only from different orbital hybridizations of carbon but also from various geometries. Nanoporous carbons have sparked high scientific interest due to their remarkable surface area and abundant nanopores, which are attractive features for applications ranging from hydrogen storage to adsorptive separations.^[1–3] Recent work reported a relatively high level of hydrogen uptake of 0.8 wt% in ultramicroporous carbon (UMC) at 25 °C and 2 MPa.^[1] This property is believed to originate from narrow

pores centered at a size of ≈ 0.5 nm,^[4,5] which is consistent with the theoretical optimum pore size between 0.6 and 0.7 nm.^[6–8] Because of the disordered, three-dimensional nature of the bulk materials, an accurate representation of the local structure and defect content, critical for understanding the adsorption performance of nanoporous carbon and for further material design, requires information that can only be obtained through atomic-resolution electron microscopy. Herein, we report a scanning transmission electron microscopy (STEM) investigation of two nanoporous carbon materials: wood-based UMC and poly(furfuryl alcohol)-derived carbon (PFAC).

Local structures of nanoporous carbon materials have been studied previously,^[9–13] yet the link between atomic-scale structure and measurable bulk properties remains elusive. Suggested local structures range from highly ordered “slit pores”, consisting of parallel graphitic planes, to glasslike structures with a global amorphous state.^[9–11] Intermediate versions have been suggested, such as a fullerene-related building block made up of graphene fragments with local curvatures caused by randomly arranging five- and seven-fold rings in the hexagonal network.^[12,13] Such a model could explain the microporosity of the carbon and many of its properties. Indeed, a recent aberration-corrected microscopy study has provided evidence of the presence of pentagonal carbon rings.^[14] Herein, we show that for the two nanoporous carbons we investigated, their three-dimensional structure

Dr. J. Guo, Prof. J. R. Morris, Dr. C. I. Contescu,
Dr. N. C. Gallego, Prof. G. Duscher,
Dr. S. J. Pennycook, Dr. M. F. Chisholm
Materials Science and Technology Division
Oak Ridge National Laboratory
Oak Ridge, TN 37831-6065, USA
E-mail: chisholmmf@ornl.gov

Dr. J. Guo, Prof. J. R. Morris, Dr. Y. Ihm,
Prof. G. Duscher, Dr. S. J. Pennycook
Department of Materials Science and Engineering
University of Tennessee
Knoxville, TN 37996, USA

DOI: 10.1002/sml.201200894



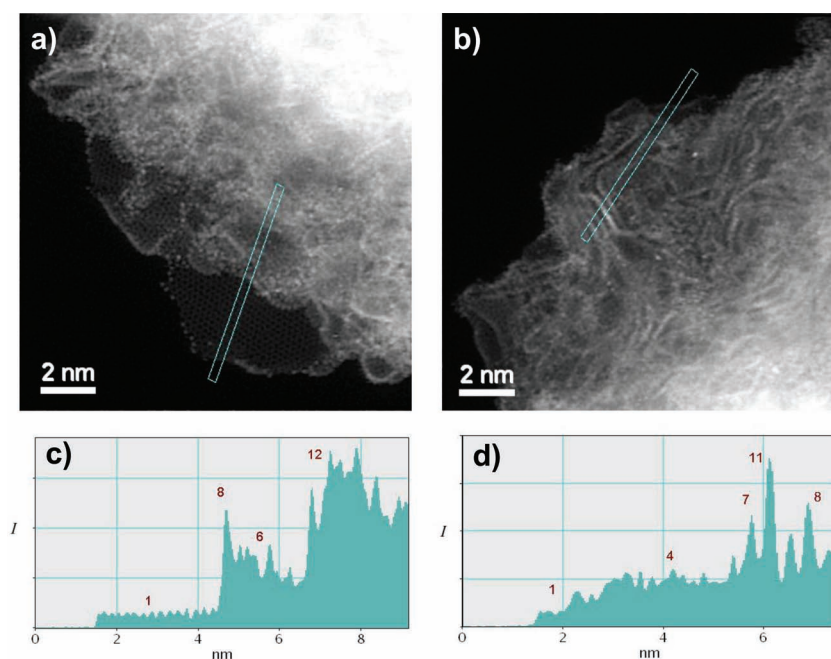


Figure 1. ADF images obtained from thinner edge areas of UMC (a) and PFAC (b). There is a variation in intensities across the image because of the changes in sample thickness. The images show the presence of a dense network of nanometer-scale pores surrounded by highly curved, predominantly single-layer carbon. The intensity profiles of UMC (c) and PFAC (d) show the carbon numbers contained in each fringe.

does indeed comprise graphene sheets containing connected five- and seven-atom ring defects. Combined with atomic-level simulation, the results show that nonhexagonal defects in graphene sheets give rise to sheet corrugation and consequently affect the stacking of graphitic layers, which in turn determines macroscopically measurable properties such as specific surface area and pore volume distribution.

2. Results and Discussion

Small crushed particles of both nanoporous carbon samples often had very thin (down to a single carbon layer) regions at their edges. Annular dark-field (ADF) images obtained from the edge area of UMC (Figure 1a) and PFAC (Figure 1b) indicate that these nanoporous carbon materials are composed of layers of relatively well ordered carbon atoms. The lines visible in the images obtained by aberration-corrected STEM are the edge-on view of individual carbon-atom planes. One can see that the nanoporous carbon materials are characterized by numerous randomly curved atom-thick carbon layers. These layers form a three-dimensional network of pores with extremely small size. Very small patches of stacked layers with lengths less than 2 nm can be occasionally observed. The gaps between the parallel planes are substantially

larger than 0.335 nm, the (0002) planar spacing of graphite,^[15] which presumably reflects the presence of a high density of slit-shaped pores or channels that have long been attributed to nanoporous carbon. For weakly scattering materials such as graphene, the image intensity is directly proportional to the number of carbon atoms under the beam.^[16] We estimated the numbers of carbon atoms contained in each bright fringe seen in Figure 1. As shown in the sectional profiles of thin areas in UMC (Figure 1c) and PFAC (Figure 1d), the fringes have higher intensities than the single-layer area, which means more carbon atoms. The brightest fringes with atom numbers slightly larger than 10 indicates that the fragment along the beam direction is less than 5 nm. The lateral extent of the graphene sheets near the edge has a similar dimension, which indicates that nanoporous carbon materials have isotropic three-dimensional networks of graphene sheets.

Further evidence that the thicker regions are composed of these single layers of well-ordered carbon atoms comes from

electron energy loss spectroscopy (EELS). Figure 2 shows EELS spectra of the carbon K-edges obtained from regions of varying thickness in both the UMC and PFAC materials. No changes in the spectrum are seen between the single layers, few-layer regions, and thick regions of the samples. In all cases, the sharp π^* peak at 285 eV followed by the σ^* peak at ≈ 292 eV and above are observed. The presence of amorphous carbon or sp^3 -bonded carbon would be expected to depress both the sharp π^* peak and the peak at the leading edge of the σ^* peak. These features are in good agreement with the previously reported spectra recorded from graphite and graphene.^[17,18] The π^* peak at 285 eV is associated with the presence of sp^2 -bonded carbon in both UMC and PFAC. It is seen that this sharp π^* peak and the peak at the leading edge of the σ^* peak do not change appreciably with

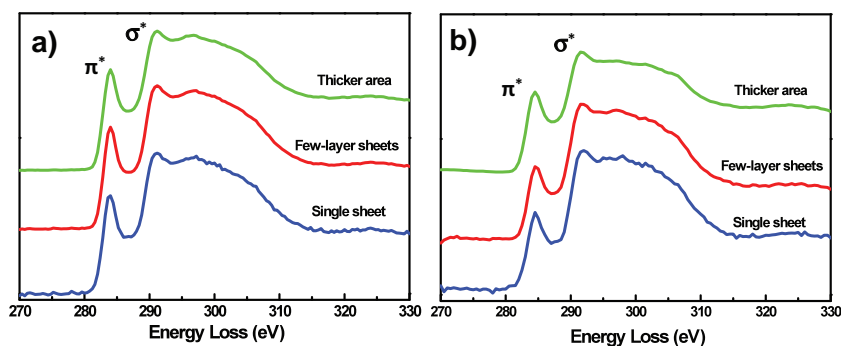


Figure 2. EELS carbon K-edges obtained from regions of varying thickness in UMC (a) and PFAC (b). No differences in the spectrum are seen between the single layers, few-layer regions, and thick regions of the samples.

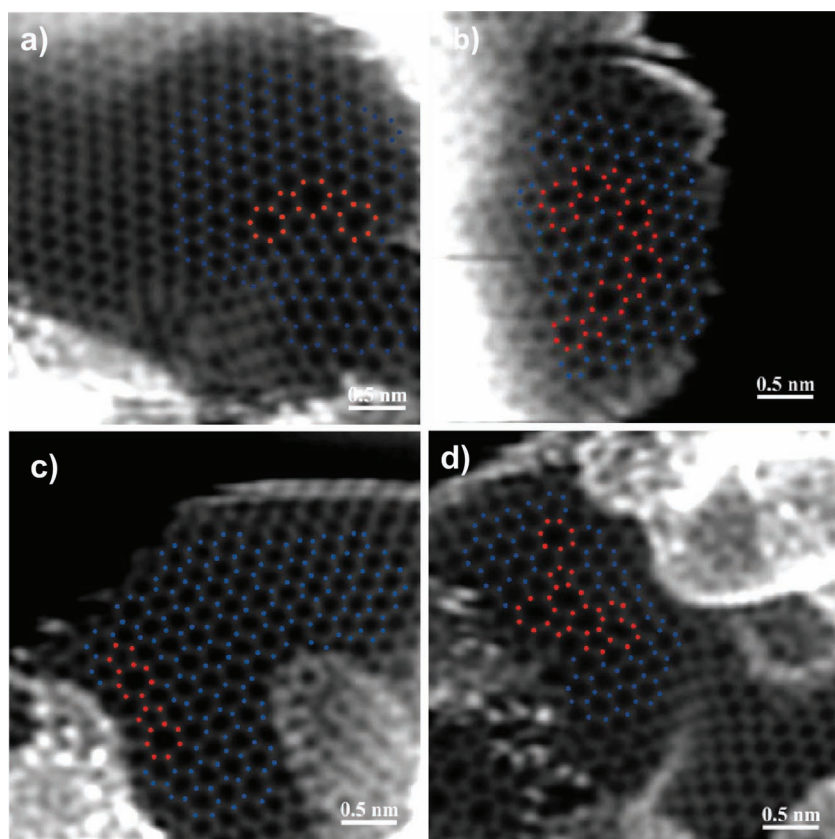


Figure 3. ADF STEM images of UMC (a,b) and PFAC (c,d) processed to remove high-frequency noise and probe tail effects. The in-plane carbon atoms are clearly resolved, and large areas of hexagonal lattice (marked in blue) with a few five- and seven-atom ring defects (marked in red) can be seen.

thickness, which indicates that these two nanoporous carbons are homogeneous and constructed from the same sp^2 -bonded carbon building block.

Over a hundred images revealing the atomic structure of single-layer areas were recorded. The results reveal the structural details of the building blocks comprising these nanoporous carbons. After processing to remove high-frequency noise and probe tail effects,^[16] the in-plane carbon atoms are clearly resolved as shown in **Figure 3**. Atomic-resolution images of nearly two-dimensional regions in UMC (Figure 3a,b) and PFAC (Figure 3c,d) reveal that the nanoporous carbons consist of curved, defective graphene sheets. That is, the building blocks are composed mostly of the hexagonal lattice of carbon with nonhexagonal defects. From Figure 3, these defects are identified as five- or seven-atom ring defects (colored in red). Indeed, at this scale, the materials are very similar. The defects are dominated by energetically favorable adjacent five- to seven-ring pairs, which form a dislocation core in the graphene structure. Moreover, these defects are highly correlated with each other, typically being found within one or two rings of another five- to seven-ring pair structure. This is similar to what has been observed in grain boundaries, where the dislocation cores align to minimize their strain energy.^[19] In addition, the carbon layers in the edge area are often seen to contain localized ripples (especially obvious in the bottom right corner of Figure 3d). These ripples in the

defective graphene layers must result in irregularly shaped pores in the bulk material. The very thin regions also reveal small patches of stacked layers each with their *c*-axis roughly parallel to the electron beam (Figure 3c,d). Graphitic stacking of these layers was not seen in our recorded images. Instead, the layers are randomly rotated. This conclusion is also supported by pair distribution function characterization using X-ray and neutron scattering, which showed limited in-plane coherence (about 1.4 nm) and incoherent stacking of graphene layers in UMC.^[20]

The UMC and PFAC materials appear to be indistinguishable at the atomic scale. However, images at slightly lower magnification of thin areas of these materials do show differences. As seen in **Figure 4**, the most obvious difference in both the ADF and bright-field (BF) images of these materials is the areal density of regions of curved and twisted, but roughly parallel lines representing the edge-on view of stacked defective graphene layers. The bright features in the ADF images arise from a locally higher atomic density that would indicate layers viewed on edge, or the curled edges of individual layers. The images from the UMC material (Figure 4a,b) show few parallel lines in the stacks that comprise this form of nanoporous carbon,

while in the PFAC material many of the stacks are seen (Figure 4c,d) to be composed of several parallel lines. X-ray and neutron diffraction studies of these materials indicate strong disorder of stacking along the *c*-axis in PFAC and almost complete loss of coherence between stacked sheets in UMC.^[20,21] Our images show that the spatial extent of this layer stacking is very different in the two materials. The PFAC contains much larger regions of stacked layers, and shows significantly smaller surface area and pore volume than UMC. Perfect regions of coherently stacked layers close to graphite-like microstructures contribute little to surface area and porosity. On the contrary, imperfectly stacked graphenes with curled and rippled shapes increase the surface area and porosity and enhance adsorption properties. This is verified by UMC, with a smaller areal density of stacked layers, having significantly higher N_2 uptake capacity than PFAC (**Figure 5**), which indicates higher surface area and pore volume.

To understand the effect of these local structures, we simulated defective graphene sheets with similar local defect structures. To generate such a sheet, a two-dimensional arrangement of purely repulsive particles was simulated at high temperatures to generate a random structure. When quenched rapidly to a zero-force configuration, the particles are predominantly ordered, forming a triangular mesh with each particle having six nearest neighbors. However, there are grain boundaries between the ordered regions, with local

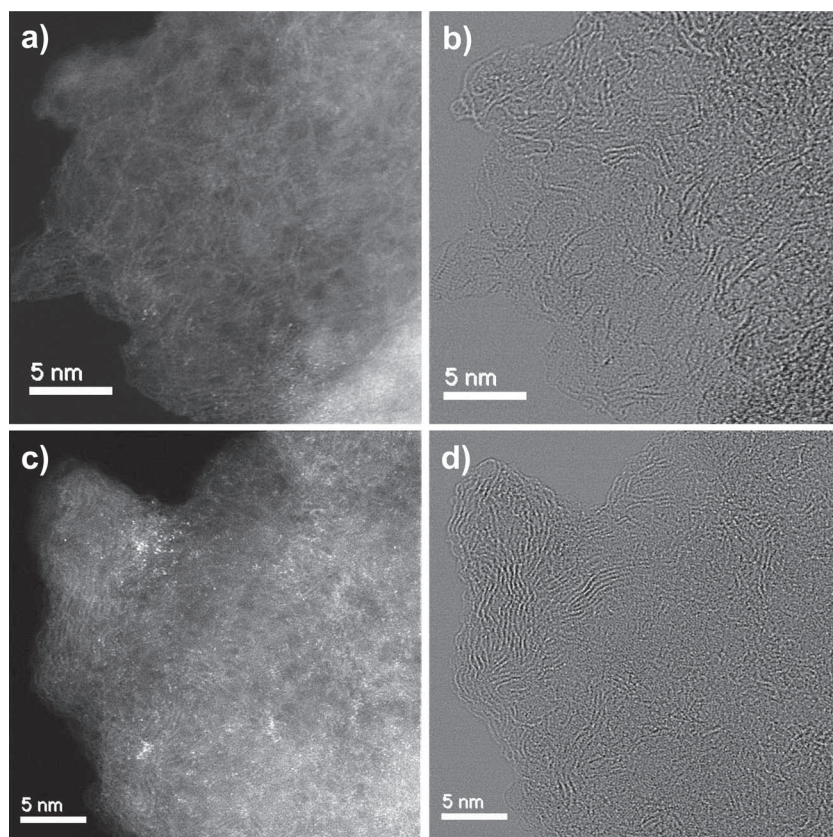


Figure 4. ADF and BF images of UMC (a,b) and PFAC (c,d). PFAC material shows more stacks of defective graphene layers than UMC material.

structures dominated by pairs of atoms with five and seven near neighbors (see figures in Reference [22] for examples). From this predominantly close-packed structure, a defective graphene sheet may be constructed by forming a “dual” of this structure, by placing a carbon atom in the center of each triangle formed by near-neighbor triplets. In this fashion, the repulsive particles with six near neighbors become the

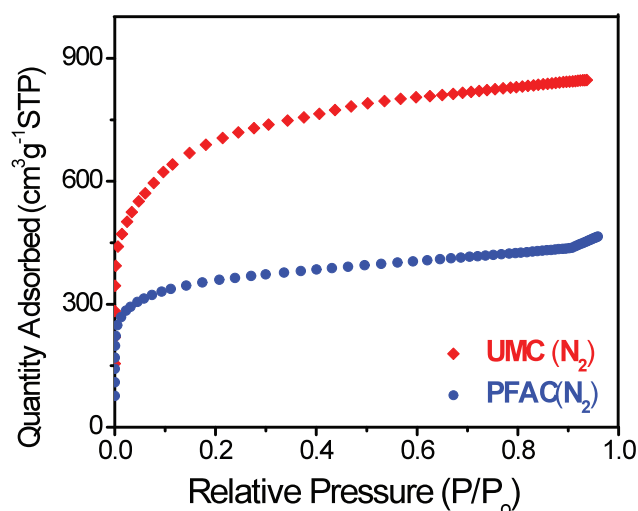


Figure 5. Nitrogen adsorption isotherms at 77 K on UMC and PFAC showing the higher N_2 uptake capacity of UMC.

centers of hexagons, and the five- and seven-coordinated atoms form five- and seven-fold rings, respectively. Equivalently, a Voronoi tessellation of this structure is formed, similar to the construction described in Reference [23]. This initially two-dimensional carbon structure was then fully relaxed by molecular dynamics, using the Tersoff interatomic potential.^[24] A section of such a sheet (with a total of 20 000 atoms) is shown in **Figure 6**. In this construction, the five- and sevenfold cores typically occur together and are highly correlated. As can be seen in Figure 6a, the local structures are clearly similar to what we observed under the microscope. The colors of the carbon atom rings correspond to atomic energies, with blue indicating the lowest and red the highest. It is easily observed that the local defects have higher energies than the hexagonal rings. This is reasonable, since the solid is not at its thermodynamic minimum as a result of the pyrolysis process.

The fully relaxed three-dimensional structure is shown in Figure 6b. As can be seen, significant distortions occur near the defect areas in the graphene sheet. While individual five- and seven-fold rings are topological defects causing local positive and negative curvature, adjacent five- and seven-fold cores do not contribute to the macroscopic curvature, but cause significant local distortions.^[25,26] This is consistent with previous reports^[27,28] showing that arrays of local cores can produce “folds” in the lattice in addition to typical grain boundary rotations. Accordingly, random localized ripples in the hexagonal network of carbon atoms, which are clearly seen in our microscope images as shown in Figure 3, would destroy the stacking of graphene fragments, thus leading to irregularly shaped nanopores and nanochannels.

Hydrogen adsorption at 25 °C and 2 MPa measured by a gravimetric method on UMC reaches 0.8 wt%, which is much higher than the 0.2 wt% on PFAC.^[21] To explore the effect of the topological defects on the adsorption ability, the H_2 adsorption energy was calculated at different positions. As shown in **Figure 7a**, a “geographic map” (with red atoms being lowest and blue atoms highest) clearly shows the “folds” in a relaxed defective graphene sheet. Locally, these distortions in the graphene sheet create favorable physisorption sites, identified by calculating the H_2 adsorption energy at different positions using a H_2 -C potential developed based on quantum chemistry calculations^[29] (see comments on the parameters for this potential in Reference [6]). In Figure 7b, we show sites for H_2 molecules where the adsorption energies are greater than 80 meV molecule⁻¹ (up to ≈ 120 meV molecule⁻¹), that is, binding strengths in excess of 900 K. These are clearly located in “folds” where the adsorbed molecules can interact with more carbon atoms. In contrast, the flatter regions show no such strong adsorption, typically with

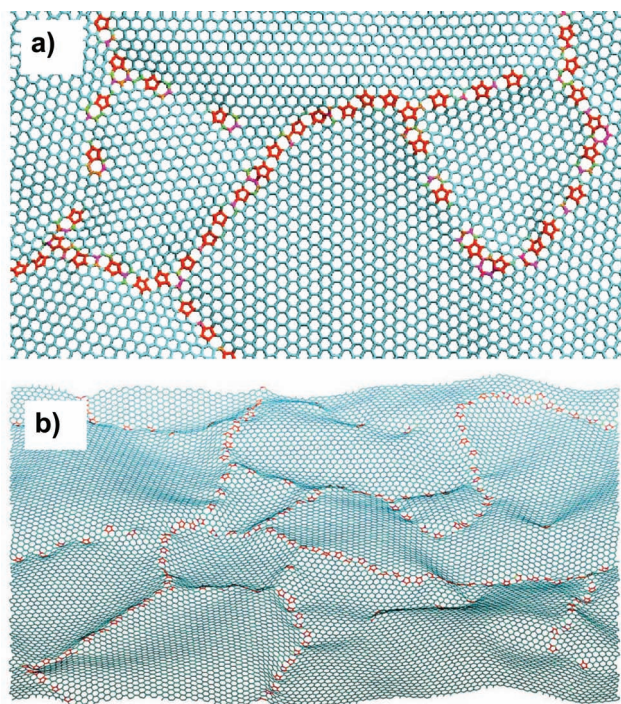


Figure 6. Segment of a simulated defective graphene sheet, with five to seven dislocation structures arranged similarly to microscopy observations. Colors indicate atomic energies, with blue representing the lowest and red the highest. a) Close-up of a region, projected along the z-axis (perpendicular to the initial plane of the unrelaxed structure). b) The entire periodic simulation cell, oriented at an angle to show the height variations.

adsorption energy between 60 and 70 meV molecule⁻¹. Such weak binding of H₂ on individual graphene sheets cannot support significant storage at ambient temperature.

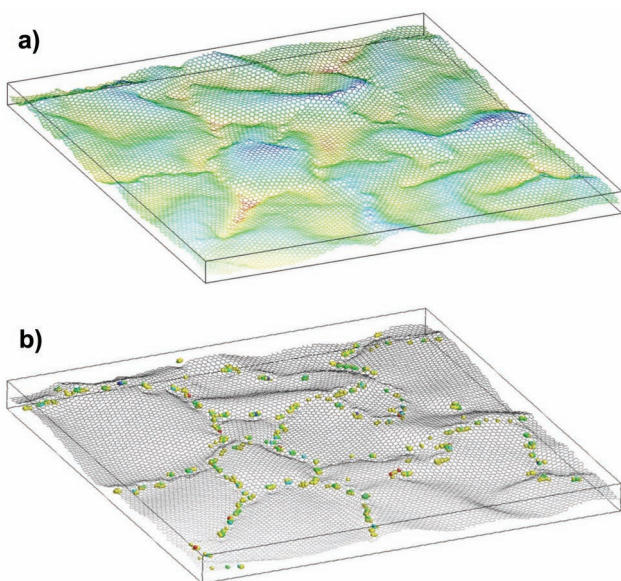


Figure 7. a) Relaxed structure of simulated defective graphene sheet. Colors indicate height (red = lowest, blue = highest). b) The same sheet, with areas of strongest H₂ adsorption indicated by colored spheres. Only areas with adsorption energies stronger than 80 meV molecule⁻¹ are shown.

Indirectly, the local distortions of each individual sheet limit the “packing” of the sheets, that is, they cannot pack as well as perfect graphene sheets. Larger distortions of the sheets will presumably interfere with the packing, assuming that defects in one sheet are uncorrelated with the next. While the typical graphite interlayer spacing is too close to permit hydrogen adsorption, some adsorption would be possible if the interlayer spacing between graphene sheets is thus expanded due to the distortions.^[6,29] The as-formed voids between graphene sheets, which are the most noticeable feature of nanoporous carbon, are therefore physisorption sites for hydrogen storage.^[30] Thus, the localized rippling induced by topological defects influences the stacking of the graphene sheets and therefore affects the porosity and H₂ adsorption performance of the nanoporous carbon materials. A similar trend is expected for physisorption of other small molecules (such as N₂, CH₄, and CO₂) under supercritical conditions.

3. Conclusion

In conclusion, we have investigated the atomic structure and defect configurations of UMC and PFAC nanoporous carbons by aberration-corrected STEM and have demonstrated that their building blocks are randomly wrinkled graphene sheets. The observed nonhexagonal defect rings of carbon atoms produce curvature of the graphene sheets, which expands the average interplanar spacing by approximately 10% and creates nanopores. Accordingly, the adsorption performance of nanoporous carbon is strongly affected by these defects. The two nanoporous carbons we observed show very different spatial extents of the stacked defective graphene sheets. The smaller these regions are, the larger the surface area and porosity measured by gas adsorption. These results imply that limiting the size of the stacked defective graphene sheets, perhaps through doping of edge sites, could further enhance the porosity of nanoporous carbons.

4. Experimental Section

The two kinds of nanoporous carbons studied herein were derived from different carbon sources. UMC is a wood-based activated carbon that has a high surface area ($S_{\text{BET}} = 2540 \text{ m}^2 \text{ g}^{-1}$) and high pore volume ($V_{\text{tot}} = 1.42 \text{ cm}^3 \text{ g}^{-1}$). PFAC was obtained by pyrolysis of the synthetic polymer poly(furfuryl alcohol) and has lower surface area and pore volume than UMC ($S_{\text{BET}} = 1530 \text{ m}^2 \text{ g}^{-1}$; $V_{\text{tot}} = 0.99 \text{ cm}^3 \text{ g}^{-1}$). Details of the synthesis procedure and additional information on properties can be found elsewhere.^[1,2,21] N₂ adsorption was performed at 77 K with an Autosorb 1C instrument from Quantachrome Corp.

The two nanoporous carbons were characterized by ADF imaging and EELS using an aberration-corrected scanning transmission electron microscope. Specimens were prepared for electron microscopy by grinding particles of the nanoporous carbon in ethanol and depositing the crushed particles onto holey carbon support films. The microstructures were studied using a Nion-UltraSTEM100 instrument operating at a low accelerating voltage of 60 kV (below the knock-on threshold of sp²-bonded carbon in

graphene^[16,31,32]). The achievable spatial resolution using this fifth-order aberration-corrected microscope at 60 kV was ≈ 1.1 Å.

Acknowledgements

This work was supported by the Materials Sciences and Engineering Division of the Office of Basic Energy Sciences, U.S. Department of Energy. This research used facilities provided by Oak Ridge National Laboratory's ShaRE User Facility, which is sponsored by the Scientific User Facilities Division, Office of Basic Energy Sciences, U.S. Department of Energy, and by the National Energy Research Scientific Computing Center, supported by the Office of Science, U.S. Department of Energy under Contract No. DEAC02-05CH11231.

- [1] V. V. Bhat, C. I. Contescu, N. C. Gallego, F. S. Baker, *Carbon* **2010**, *48*, 1331–1340.
- [2] C. L. Burket, R. Rajagopalan, A. P. Marenic, K. Dronvajjala, H. C. Foley, *Carbon* **2006**, *44*, 2957–2963.
- [3] M. Acharya, M. S. Strana, J. P. Mathews, S. J. L. Billinge, V. Perkov, S. Subramoney, H. C. Foley, *Philos. Mag. B* **1999**, *79*, 1499–1518.
- [4] M. B. Rao, S. Sircar, *J. Membr. Sci.* **1996**, *110*, 109–118.
- [5] R. K. Mariwala, H. C. Foley, *Ind. Eng. Chem. Res.* **1994**, *33*, 2314–2321.
- [6] R. S. Aga, C. L. Fu, M. Krmar, J. R. Morris, *Phys. Rev. B* **2007**, *76*, 165404.
- [7] I. Cabria, M. J. Lopez, J. A. Alonso, *Carbon* **2007**, *45*, 2649–2658.
- [8] P. Kowalczyk, H. Tanaka, R. Hołyst, K. Kaneko, T. Ohmori, J. Miyamoto, *J. Phys. Chem. B* **2005**, *109*, 17174–17183.
- [9] D. M. Ford, E. D. Glandt, *J. Phys. Chem.* **1995**, *99*, 11543–11549.
- [10] H. F. Stoeckli, *Carbon* **1990**, *28*, 1–6.
- [11] L. Hawelek, A. Brodka, J. C. Dore, V. Honkimaki, A. Burian, *Diamond Relat. Mater.* **2008**, *17*, 1633–1638.
- [12] P. J. F. Harris, A. Burian, S. Duber, *Philos. Mag. Lett.* **2000**, *80*, 381–386.
- [13] P. J. F. Harris, S. C. Tsang, *Philos. Mag. A* **1997**, *76*, 667–677.
- [14] P. J. F. Harris, Z. Liu, K. Suenaga, *J. Phys.: Conference Series* **2010**, *241*, 012050.
- [15] J. J. Guo, G. H. Liu, X. M. Wang, T. Fujita, B. S. Xu, M. W. Chen, *Appl. Phys. Lett.* **2009**, *95*, 051920.
- [16] O. L. Krivanek, M. F. Chisholm, V. Nicolosi, T. J. Pennycook, G. J. Corbin, N. Dellby, M. F. Murfitt, C. S. Own, Z. S. Szilagyí, M. P. Oxley, S. T. Pantelides, S. J. Pennycook, *Nature* **2010**, *464*, 571–574.
- [17] K. A. Mkhoyan, A. W. Contryman, J. Silcox, D. A. Stewart, G. Eda, C. Mattevi, S. Miller, M. Chhowalla, *Nano Lett.* **2009**, *9*, 1058–1063.
- [18] K. Suenaga, M. Koshino, *Nature* **2010**, *468*, 1088–1090.
- [19] P. Y. Huang, C. S. Ruiz-Vargas, A. M. Van der Zande, W. S. Whitney, M. P. Levendorf, J. W. Kevek, S. Garg, J. S. Alden, C. J. Hustedt, Y. Zhu, J. Park, P. L. McEuen, D. A. Muller, *Nature* **2011**, *469*, 389–392.
- [20] W. Dmowski, C. I. Contescu, A. Llobet, N. C. Gallego, T. Egami, *J. Phys. Chem. C* **2012**, *116*, 2946–2951.
- [21] C. I. Contescu, D. Saha, N. C. Gallego, E. Mamontov, A. I. Kolesnikov, V. V. Bhat, *Carbon* **2012**, *50*, 1071–1082.
- [22] F. H. Stillinger, T. A. Weber, *Phys. Rev. A* **1982**, *25*, 978–989.
- [23] D. R. Nutt, H. Weller, *J. Chem. Theory Comput.* **2009**, *5*, 1877–1882.
- [24] J. Tersoff, *Phys. Rev. Lett.* **1988**, *61*, 2879–2882.
- [25] A. Hashimoto, K. Suenaga, A. Gloter, K. Urita, S. Iijima, *Nature* **2004**, *430*, 870–873.
- [26] F. Banhart, J. Kotakoski, A. V. Krasheninnikov, *ACS Nano* **2010**, *5*, 26–41.
- [27] M. T. Lusk, L. D. Carr, *Phys. Rev. Lett.* **2008**, *100*, 175503.
- [28] Y. Y. Liu, B. Yakobson, *Nano Lett.* **2010**, *10*, 2178–2183.
- [29] S. Patchkovskii, J. S. Tse, S. N. Yurchenko, L. Zhechkov, T. Heine, G. Seifert, *Proc. Natl. Acad. Sci. USA* **2005**, *102*, 10439–10444.
- [30] N. Texier-Mandoki, J. Dentzer, T. Piquero, S. Saadallah, P. David, C. Vix-Guterl, *Carbon* **2004**, *42*, 2744–2747.
- [31] A. V. Krasheninnikov, F. Banhart, *Nat. Mater.* **2007**, *6*, 723–733.
- [32] A. Zobelli, A. Gloter, C. P. Ewels, G. Seifert, C. Colliex, *Phys. Rev. B* **2007**, *75*, 245402.

Received: April 25, 2012
 Revised: June 14, 2012
 Published online: August 14, 2012